# Absolute Metal−Ligand $\sigma$ Bond Enthalpies in Group 4 Metallocenes. A Thermochemical, Structural, Photoelectron Spectroscopic, and ab Initio Quantum Chemical Investigation

**Wayne A. King,[†] Santo Di Bella,[‡] Antonino Gulino,[‡] Giuseppe Lanza,[§] Ignazio L. Fragalà,*[,‡] Charlotte L. Stern,[†] and Tobin J. Marks*[,†]**

*Contribution from the Department of Chemistry, Northwestern University, Evanston, Illinois 60208-8113, Dipartimento di Scienze Chimiche, Università di Catania, 95125 Catania, Italy, and Dipartimento di Chimica, Università della Basilicata, 85100 Potenza, Italy*

*Received June 29, 1998*

**Abstract:** Absolute metal−ligand $\sigma$ bond enthalpies have been determined for a series of titanocene, zirconocene, and hafnocene halides and dimethyls by iodinolytic titration calorimetry. Absolute metal−iodine bond disruption enthalpies were measured by iodination of the monomeric trivalent group 4 metallocenes $Cp^{tt}_2TiI$, $(Me_5C_5)_2$-TiI, $Cp^{tt}_2ZrI$, and $Cp^{tt}_2HfI$ ($Cp^{tt} = \eta^5$-1,3-di-*tert*-butylcyclopentadienyl). Iodinolysis of $Cp^{tt}_2ZrMe_2$ and $Cp^{tt}_2HfMe_2$ in turn yields absolute Zr−Me and Hf−Me bond enthalpies. Derived values (kcal/mol) are $D[Cp^{tt}_2Ti(I)-I] = 40.6(5)$; $D[(Me_5C_5)_2Ti(I)-I] = 52.3(6)$; $D[Cp^{tt}_2Zr(I)-I] = 58.0(5)$; $D[Cp^{tt}_2Hf(I)-I] = 61.2(4)$; $\bar{D}[Cp^{tt}_2Zr\text{-}Me_2] = 43(1)$; and $\bar{D}[Cp^{tt}_2Hf-Me_2] = 47.6(9)$. That $D[Cp^{tt}_2Zr(I)-(I)] \approx D(I_3Zr-I)$ and $D[(Me_5C_5)_2$-$Ti(I)-I] \approx D(I_3Ti-I)$, while $D[Cp^{tt}_2Ti(I)-I] \approx D(I_3Ti-I) - 12$ kcal/mol, argues for more reliable transferability of $D(M^{IV}-I)$ in sterically less congested metallocenes. The molecular structures of $Cp_2{}^{tt}ZrI_2$, $Cp_2{}^{tt}ZrI$, and $Cp_2$ttHfI were determined by X-ray diffraction. In $Cp^{tt}_2ZrI_2$, the Zr ligation is pseudotetrahedral, and the ring *tert*-butyl groups "straddle" the Zr−I bonds to minimize steric interactions. The geometry about Zr in $Cp^{tt}_2ZrI$ is pseudotrigonal, with *contracted* Zr−ring centroid and Zr−I distances versus $Cp^{tt}_2ZrI_2$, primarily reflecting substantially diminished ligand−ligand repulsive nonbonded interactions in the latter. $Cp^{tt}_2HfI$ is isomorphous with $Cp^{tt}_2ZrI$, and the slightly different metrical parameters are in accord with Hf vs Zr ionic radii. The significant differences in interligand repulsive interactions in the trivalent versus tetravalent complexes are confirmed by van der Waals calculations. High-resolution UV PE spectra combined with ab initio relativistic effective core potential calculations provide details of electronic structure. Absolute ionization energy values indicate that iodine behaves as both a strong $\sigma$ and $\pi$ donor. Trends in the large $Cp_2MX_n$ structural database can be understood in terms of the interplay between electronic and molecular structure factors, which are highly sensitive to the substitution patterns of the cyclopentadienyl ligands and, in particular, to competing $\sigma$ vs $\pi$ M−X bonding.

## Introduction

Group 4 metallocenes are pivotal reagents in a myriad of useful and instructive stoichiometric and catalytic transformations. A full understanding of this chemistry necessarily requires a quantitative assessment of the strengths of bonds being made and broken in such transformations. To date, a substantial bonding energetic knowledge base for group 4 metallocenes has been acquired by solution thermochemical measurements.[1,2] However, while quantities such as $D[L_2M(X)-X]$ have been measured for L = a variety of ancillary $\eta^5$-cyclopentadienyl ligands and X = a variety of $\sigma$-bonded ligands, the results have necessarily and pragmatically been "anchored" to the corresponding bond enthalpy values of the corresponding tetrahalides. This approach reflects the paucity of measured absolute $D[L_2M(X)-X]$ values and implicitly assumes a reasonable but as yet incompletely tested transferability of D(M−X) from one environment to the other.

Typical solution calorimetric approaches to evaluating metallocene metal−ligand bond enthalpies[1,2] have involved the reaction of metal complexes with oxidants or Brønsted acids (eq 1). Such reactions do not, however, provide absolute

$$L_nMR + AB \rightarrow L_nMA + BR \qquad (1)$$

($L_n$ = ancillary ligands, AB = oxidant or Brønsted acid)

measurements unless one constituent bond enthalpy is known absolutely.[3] Alternatively, absolute enthalpies can be measured

[†] Northwestern University.
[‡] Università di Catania.
[§] Università della Basilicata.

(1) (a) Hoff, C. D. *Prog. Inorg. Chem.* **1992**, *40*, 503−561. (b) Marks, T. J., Ed. *Bonding Energetics in Organometallic Compounds*; ACS Symposium Series 428; American Chemical Society: Washington, DC, 1990. (c) Martino Simoes, J. A.; Beachamp, J. L. *Chem. Rev.* **1990**, *90*, 629−688 (d) Marks, T. J., Ed. *Metal−Ligand Bonding Energetics in Organo-Transition Metal Compounds;* Polyhedron Symposium-in-Print 7; Elsevier: New York, 1988.

(2) (a) Skinner, H. A.; Connor, J. A. In *Molecular Structure and Energetics*, Vol. 2; Liebman, J. F., Greenberg, A., Eds.; VCH Publishers: New York, 1987; Chapter 6. (b) Skinner, H. A.; Connor, J. A. *Pure Appl. Chem.* **1985**, *57*, 79−88. (c) Pearson, R. G. *Chem. Rev.* **1985**, *85*, 41−59. (d) Mondal, J. V.; Blake, D. M. *Coord. Chem. Rev.* **1983**, *47*, 204−238. (e) Mansson, M. *Pure Appl. Chem.* **1983**, *55*, 417−426. (f) Halpern, J. *Acc. Chem. Res.* **1982**, *15*, 238−244. (g) Pilcher, G.; Skinner, H. A. In *The Chemistry of the Metal−Carbon Bond*; Hartley, F. R., Patai, S., Eds.; Wiley: New York, 1982; pp 43−90. (h) Connor, J. A. *Top. Curr. Chem.* **1977**, *71*, 71−110. (i) McMillen, D. F.; Golden, D. M. *Annu. Rev. Phys. Chem.* **1982**, *33*, 493−532. (j) Dean, J. A. *Handbook of Organic Chemistry*; McGraw-Hill: New York 1987; pp 3-19−3-27.

10.1021/ja9822815 CCC: $18.00 
Published on Web 01/05/1999

via oxidative addition of an appropriate ligand reagent to a related low-valent parent complex (e.g., eq 2). This latter

$$L_nM + {}^1/_2X_2 \rightarrow L_nMX \qquad (X = I, OR, SR) \qquad (2)$$

$$D(L_nM-X) = {}^1/_2D(X-X) - \Delta H_{eq\,2}$$

approach, of course, requires monomeric, lower oxidation state metal complexes and has been employed successfully for evaluating absolute metal−ligand bond enthalpies in several f-element and one early transition metal system, namely ($\eta^5$-$C_5H_4SiMe_3)_3U$,[4] ($\eta^5$-$^t$BuCp)$_3$U,[5] ($\eta^5$-indenyl)$_3$U,[5] $(Me_5Cp)_2Ln$ (Ln = Eu,[6] Yb,[6] Sm[7]), and $(Me_5Cp)_2TiCl$.[8]

In the same perspective, the successful recent stabilization of *monomeric trivalent* group 4 $Cp^{tt}_2MCl$ complexes[9] using the bulky $Cp^{tt}$ ligand ($Cp^{tt}$ = $\eta^5$-1,3-$^t$Bu$_2$Cp) affords a unique opportunity to quantify absolute group 4 metallocene metal−ligand $\sigma$ bond enthalpies as expressed in eq 3. This would help

$$Cp_2MI_2 \rightarrow Cp_2MI + I \qquad (3)$$

to place the existing database on an absolute basis and test the aforementioned transferability relationships. In this contribution, we report on new, efficient synthetic routes to $Cp^{tt}_2ZrI_2$, $Cp^{tt}_2HfI_2$, $Cp^{tt}_2ZrI$, and $Cp^{tt}_2HfI$ metallocenes, as well as on crystallographic studies of $Cp^{tt}_2ZrI_2$, $Cp^{tt}_2ZrI$, and $Cp^{tt}_2HfI$, which allow detailed analysis of the molecular structure reorganizations accompanying homolytic eq 3. We also report absolute M−I bond enthalpy measurements in the complexes $Cp^{tt}_2MI_2$ (M = Ti, Zr, Hf) and $(Me_5C_5)_2TiI_2$, as well as measurements of metal−methyl bond enthalpies in $Cp^{tt}_2ZrMe_2$ and $Cp^{tt}_2HfMe_2$, the syntheses of which offer an expedient route to the homologous iodides. These determinations allow comparison with D(M−I)/D(M−Me) data on related $(Me_5Cp)_2$ and $Cp_2$ homologues[10] and, it will be seen, evaluation of effects due to the more sterically encumbered ancillary ligation. Furthermore, these experimental observations are placed in perspective by analysis of $Cp^{tt}_2ZrI$, $Cp^{tt}_2ZrI_2$, and $Cp^{tt}_2ZrCl_2$ electronic structure using combined ab initio quantum chemical calculations and experimental gas-phase He I/He II photoelectron spectroscopy, as well as by theoretical evaluation of the absolute metal−ligand bond enthalpies and intramolecular repulsive interactions.

(3) The metal−ligand bond disruption enthalpy $D(L_nM-R)$ is defined for the adiabatic homolytic processes of eqs a and b,[1,2] where all species are assumed to be in electronically and geometrically relaxed states.

$$L_nM-R \rightarrow L_nM + R\cdot \qquad (a)$$

$$D(L_nM-R) = \Delta H_f^\circ(L_nM) + \Delta H_f^\circ(R\cdot) - \Delta H_f^\circ(L_nM-R) \qquad (b)$$

$$D(L_nM-R) - D(L_nM-A) = \Delta H_{eq\,1} - D(A-B) + D(B-R) \qquad (c)$$

(4) Schock, L. E.; Seyam, A. M.; Marks T. J. In ref 1d, pp 1517−1530.
(5) Jemine, X.; Goffart, J.; Berthet, J.; Ephritikhine, M. *J. Chem. Soc., Dalton Trans.* **1992**, 2439−2440.
(6) Nolan, S. P.; Stern, D.; Hedden, D.; Marks, T. J. In ref 1b, pp 159−174.
(7) Nolan, S. P.; Stern, D.; Marks T. J. *J. Am. Chem. Soc.* **1989**, *111*, 7844−7853.
(8) Dias, A. R.; Salema, M. S.; Martinho Simoes, J. A.; Pattiasina, J. W.; Teuben, J. H. *J. Organomet. Chem.* **1988**, *346*, C4−C6.
(9) (a) Urazowski, I. F.; Ponomaryov, I. V.; Ellert, O. G.; Nifant'ev, I. E.; Lemenovskii, D. A. *J. Organomet. Chem.* **1988**, 356, 181−193. (b) Urazowski, I. F.; Ponomaryov, I. V.; Nifant'ev, I. E.; Lemenovskii, D. A. *J. Organomet. Chem.* **1989**, *368*, 287−294.
(10) Schock, L. E.; Marks T. J. *J. Am. Chem. Soc.* **1988**, *110*, 7701−7715.

## Experimental Section

**General Considerations.** All manipulations were carried out under purified argon or nitrogen using glovebox and standard high-vacuum line or Schlenk techniques. Solvents were predried and distilled as appropriate. Toluene for calorimetric measurements was additionally stored over Na/K alloy and vacuum transferred immediately prior to use. Iodine was sublimed prior to use. Dichloromethane was purified by stirring over $P_2O_5$, freeze−thaw degassing, and vacuum transferring prior to use. Hg was degassed and dried by heating under high vacuum prior to use. $^1$H NMR spectra were recorded on Varian XL-400 (400 MHz) or Gemini (300 MHz) spectrometers and referenced to $SiMe_4$ unless otherwise indicated.

**Syntheses.** The reagents 1,3-di-*tert*-butylcyclopentadiene (**1**)[11] and $(Me_5Cp)_2TiI$ (**2**)[12] were prepared according to literature procedures.

**NaCp$^{tt}$ (3).** Sodium hydride (14.0 g, 0.588 mol) was suspended in 500 mL of THF. Reagent **1** (20.3 g, 0.114 mol), previously dried over BaO, degassed, and vacuum distilled, was syringed into the sodium hydride suspension under $N_2$. The reaction mixture was allowed to stir for 3 days and filtered through Celite. The volume of the filtrate was reduced until a thick suspension resulted. Pentane (350 mL) was syringed into the suspension, and the suspension was stirred until all of the product precipitated. The supernatant was then filtered off and the resulting white solid collected and dried in vacuo. Yield: 19.4 g (85%). $^1$H NMR (THF-$d_8$): $\delta$ 1.20 (s, 18H), 5.40 (d, 2H), 5.54 (t, 1H).

**Cp$^{tt}_2$TiCl (4)**. THF (120 mL) was vacuum transferred from Na/K alloy onto a mixture of $TiCl_3$ (1.51 g, 9.79 mmol) and **3** (4.04 g, 19.6 mmol) at −78 °C. The solution was stirred and allowed to warm slowly to 10 °C overnight, during which time the color changed from purple to deep blue. The solution was then cooled to 0 °C and allowed to stir for 1 day, followed by an additional day at 25 °C. The THF was next removed in vacuo, and the blue solids were extracted with 100 mL of pentane. The resulting blue solution was filtered, and the filtrate volume was reduced by ∼75%. The solution was then slowly cooled to −78 °C, and the supernatant was decanted from the resulting blue crystalline product. The product also contained a small amount of black foamy solid. Recrystallization of the crude product at −78 °C from 20 mL of pentane yielded a clean blue crystalline product. Yield: 2.61 g (61%). An NMR scale oxidation of **4** with $CCl_4$ yielded a $^1$H NMR spectrum identical to that reported in the literature for diamagnetic $Cp^{tt}_2TiCl_2$.[9a]

**Cp$^{tt}_2$TiI (5).** Diethyl ether (75 mL) was vacuum transferred from Na/K alloy onto a mixture of **4** (1.04 g, 2.30 mmol) and LiI (3.10 g, 23.1 mmol) at −78 °C. The blue solution was then warmed to room temperature with stirring, during which time the color darkened. The reaction mixture was stirred for approximately 16 h at room temperature and then heated at reflux for 1 h. The $Et_2O$ was next removed in vacuo from the dark green solution, and the resulting solids were extracted with 50 mL of pentane. The green solution was filtered from the solids, and the pentane was removed in vacuo. The resulting product contained traces of white solid. The product was extracted again with 50 mL of pentane to remove the remaining salt, and the filtrate was concentrated and slowly cooled to −78 °C. The solvent was then decanted to yield dark green crystalline product. Yield: 0.30 g (25%). Anal. Calcd for $C_{26}H_{42}TiI$: C, 59.0; H, 8.0. Found: C, 59.2; H, 8.0.

**Cp$^{tt}_2$TiI$_2$ (6).** Complex **5** (0.447 g, 0.844 mmol) was taken up in 50 mL of toluene. Solid $I_2$ (0.202 g, 0.795 mmol) was quickly weighed out in air and added to the toluene solution under an Ar flush. The color of the reaction mixture rapidly turned from dark green to dark red-brown. The reaction mixture was stirred for 20 min. The toluene was then removed under vacuum and the product warmed to 70 °C in vacuo for 40 h to sublime out excess $I_2$. Next, 50 mL of $CH_2Cl_2$ was vacuum transferred onto the brown solid. After being stirred for ∼1 h, the mixture was filtered, and the $CH_2Cl_2$ was removed from the filtrate in vacuo. The product was then dissolved in 1 mL of $CH_2Cl_2$, and 5−10 mL of pentane was layered on top of the $CH_2Cl_2$ solution. On slow cooling of the solution to −78 °C overnight, dark red-brown crystals were isolated. Yield: 0.36 g (66%). $^1$H NMR ($C_6D_6$): $\delta$ 1.34

(11) Venier, C. G.; Casserly, E. W. *J. Am. Chem. Soc.* **1990**, *112*, 2808−2809.
(12) Pattiasina, J. W.; Heeres, H. J.; van Bolhuis, F.; Meetsma, A.; Teuben, J. H.; Spek, A. L. *Organometallics* **1987**, *6*, 1004−1010.

(s, 36H), 5.66 (d, 4H), 7.99 (t, 2H). Anal. Calcd for $C_{26}H_{42}TiI_2$: C, 47.6; H, 6.4. Found: C, 47.4; H, 6.5.

**Modified Literature Preparation[9b] of $Cp^{tt}_2ZrCl_2$ (7).** $ZrCl_4$ (4.763 g, 20.44 mmol) and **3** (8.94 g, 43.4 mmol) were refluxed in 75 mL of THF for ∼16 h. A light yellow solution formed. The THF was then removed in vacuo, and the solids were treated with 30 mL of $CH_2Cl_2$ to destroy any remaining **3**. Next, 100 mL of THF was added to the $CH_2Cl_2$ solution. After being stirred for ∼1 h, the mixture was filtered through Celite. The solvent was next removed from the filtrate in vacuo. The solids were then stirred with 50 mL of pentane for approximately 16 h, and the resulting solution was slowly cooled to −78 °C. The pentane was next decanted and the colorless crystalline product dried in vacuo. The product can be further purified by sublimation (120−180 °C/$10^{-5}$ Torr). The $^1$H NMR spectrum was identical to that reported in the literature.[9b] Yield: 6.86 g (65%).

**Modified Literature Preparation[9b] of $Cp^{tt}_2HfCl_2$ (8).** $HfCl_4$ (2.353 g, 7.346 mmol) and **3** (3.031 g, 14.71 mmol) were stirred in 75 mL of THF at room temperature for ∼16 h and then refluxed for 1 day at 80 °C. A light yellow solution resulted. The THF was next removed in vacuo, and the solid was treated with 30 mL of $CH_2Cl_2$ to destroy any remaining **3**. The $CH_2Cl_2$ was removed in vacuo, and the solids extracted with THF and filtered through Celite. The THF was then removed in vacuo from the filtrate, and the solids were stirred with 30 mL of pentane for ∼16 h. The resulting solution was slowly cooled to −78 °C, the pentane decanted, and the colorless crystalline product dried in vacuo. The $^1$H NMR spectrum was identical to that reported in the literature.[9b] The product can be further purified by sublimation (120−180 °C/$10^{-5}$ Torr). Yield: 2.72 g (62%).

**$Cp^{tt}_2HfMe_2$ (9).** MeLi (8.5 mL, 1.4 M in $Et_2O$) was syringed into an 80-mL toluene solution of **8** (1.508 g, 2.497 mmol), and the reaction mixture was stirred for 2 days at room temperature. The toluene was then removed in vacuo, and the resulting solids were extracted with 30 mL of pentane. After filtration, the volume of the filtrate was reduced until a precipitate began to form. The solution was then slowly cooled to −78 °C, and the supernatant was decanted, yielding a colorless precipitate. The product was dried in vacuo. Yield: 1.08 g (77%). $^1$H NMR ($C_6D_6$): $\delta$ 1.27 (s, 36H), $\delta$ 5.36 (d, 4H), $\delta$ 6.44 (t, 2H) $\delta$ 0.00 (s, 6H). Anal. Calcd for $C_{28}H_{48}Hf$: C, 59.7; H, 8.6. Found: C, 59.7; H, 8.6.

**$Cp^{tt}_2ZrMe_2$ (10).** This procedure was the same as that described for **9** above. The following stoichiometries were used: **7** (2.06 g, 3.98 mmol) and 10 mL of MeLi (1.4 M in $Et_2O$). Yield: 1.46 g (77%). $^1$H NMR ($C_6D_6$): $\delta$ 0.19 (s, 6H), 1.26 (s, 36H), 5.41 (d, 4H), 6.54 (t, 2H). Anal. Calcd for $C_{28}H_{48}Zr$: C, 70.7; H, 10.2. Found: C, 70.6; H, 10.2.

**$Cp^{tt}_2HfI_2$ (11).** Compound **9** (2.064 g, 3.665 mmol) was taken up in 15 mL of toluene and cooled to −78 °C. $I_2$ (2.22 g, 8.746 mmol) was dissolved in 50 mL of toluene under an Ar atmosphere. The $I_2$ solution was slowly titrated by syringe into the stirring solution of **9** under an Ar flush. Upon $I_2$ addition, the solution of **9** turned bright yellow in color and consumed the aliquot of $I_2$. The titration was continued until the $I_2$ color was no longer discharged, and the solution remained a light red. The reaction mixture was then stirred for 30 min and allowed to warm to room temperature. The solvent was removed in vacuo, and the resulting solid product was warmed to 50 °C/$10^{-5}$ Torr for 16 h to sublime out the excess $I_2$. The yellow crude product was then stirred with 20 mL of refluxing pentane for 60 min, and the solution was next cooled to room temperature and then slowly to −78 °C. The yellow crystalline product was collected by filtration, dried in vacuo for 60 min, and then sublimed (180 °C/$10^{-5}$ Torr). Yield: 2.65 g (92%). $^1$H NMR ($C_6D_6$): $\delta$ 1.34 (s, 36H), 5.65 (d, 4H), 7.20 (t, 2H). Anal. Calcd for $C_{26}H_{42}HfI_2$: C,39.7; H, 5.4. Found: C, 39.4; H, 5.2.

**$Cp^{tt}_2ZrI_2$ (12).** This procedure was performed as described for **11** above using **10** (1.728 g, 3.631 mmol). The sublimation of excess $I_2$ was carried out for 2 days at 100 °C/$10^{-5}$ Torr. The bright yellow metallocene product was purified by sublimation (120 °C/$10^{-5}$ Torr). Yield: 1.83 g (72%). $^1$H NMR ($C_6D_6$): $\delta$ 1.33 (s, 36H), 5.74 (d, 4H), 7.36 (t, 2H). Anal. Calcd for $C_{26}H_{42}ZrI_2$: C, 44.6; H, 6.0. Found: C, 44.6; H, 6.0.

**$Cp^{tt}_2HfI$ (13).** Compound **11** (1.525 g, 1.938 mmol) was dissolved in 20 mL of THF, vacuum transferred from Na/K alloy at −78 °C. The mixture was warmed until **11** was completely dissolved. The yellow solution was then cooled to −20 °C and poured onto stirring K/Hg amalgam (0.080 g K (2.0 mmol)/27.1 g Hg). A colorless precipitate immediately formed, while the supernatant remained yellow in color. Traces of **11** were washed from the addition flask with additional THF (the total volume of THF was 50−80 mL) until no more color was observed. After the addition flask was washed, the reaction mixture was allowed to warm to 0 °C and then slowly to room temperature. The total reaction time from first addition of **11** to the K/Hg amalgam was ∼4 h. The solution was then decanted from the amalgam, and the THF was removed in vacuo. Next, 30−50 mL of pentane was vacuum transferred onto the crude product, the resulting yellow solution was filtered, and the volume of the filtrate was reduced until a precipitate began to form. The solution was then slowly cooled to −78 °C, whereupon a yellow, crystalline precipitate formed. The pentane was decanted from the product, and the solid was dried in vacuo. Yield: 1.07 g (84%). Anal. Calcd for $C_{26}H_{42}HfI$: C, 47.3; H, 6.4. Found: C, 47.5; H, 6.3.

**$Cp^{tt}_2ZrI$ (14).** This procedure was performed as described for **13** above**.** The following amounts were used: **12** (0.705 g, 1.01 mmol) and K/Hg amalgam (0.041 g K (1.04 mmol)/28.9 g Hg). Yield: 0.47 g (81%). Anal. Calcd for $C_{26}H_{42}ZrI$: C, 54.5; H, 7.4. Found: C, 54.2; H, 7.1.

**$^1$H NMR Experiments for Calorimetry.** To establish that the transformations used in the calorimetry were rapid, clean, and quantitative, all iodination reactions were investigated by $^1$H NMR. In a Wilmad screw-capped NMR tube fitted with a septum, a known amount of metallocene complex (in $C_6D_6$) was reacted with a stoichiometric excess of $I_2$ solution in $C_6D_6$, injected incrementally via a gastight syringe. After each injection and vigorous shaking, the resulting solution was checked by NMR to verify completion and reaction stoichiometry. As observed by $^1$H NMR, the presence of excess of $I_2$ did not decompose the resulting metallocene diiodides.

**Titration Calorimetry.** Solution reaction calorimetry was performed in a Tronac model 450 isoperibol calorimeter extensively modified for the study of extremely air- and moisture-sensitive compounds.[4,10,13] A typical experiment was performed as follows. A metallocene solution of known concentration in toluene was prepared on the day of the experiment. For the extremely air-sensitive trivalent group 4 systems, an ampule of metallocene (20 mg) dissolved in ∼5 mL of toluene was also prepared. Furthermore, a toluene solution containing stoichiometrically excess $I_2$ was prepared on the day of the experiment. The $I_2$ and metallocene solutions were fitted to the calorimeter, and the calorimeter was evacuated and back-filled several times with Ar. The metallocene solution was then introduced into the calorimeter buret, and the ampule containing the metallocene solution was discharged into the reaction dewar as a check on the integrity of the calorimeter atmosphere. If the color of the metallocene solution bleached, no measurements were attempted. The $I_2$ solution was introduced into the reaction dewar under a slight vacuum. The system was then placed under Ar, stirring initiated, and the reaction dewar lowered into the calorimeter constant-temperature bath (25.000 ± 0.001 °C) for thermal equilibration. A series of electrical calibration runs was then performed. Next, a series of metallocene solution injections was carried out using the calibrated motor-driven buret of the calorimeter (11−20 individual injections per run). At the end of the series of titrations, a further set of electrical calibrations was performed. An experimental heat capacity was then derived from the average of the electrical calibration runs. Given the molarity of the titrant and the buret delivery rate, the enthalpy of reaction could be calculated.

**X-ray Crystallographic Studies.** All measurements were performed on an Enraf-Nonius CAD4 diffractometer at −120 °C using Mo *K*α radiation. Crystals were mounted on glass fibers using Paratone oil. All calculations were performed on a VAX11/730 computer using the TEXSAN crystallographic software package.[14] Experimental details, positional parameters, and thermal parameters for **12**, **13**, and **14** are presented in Tables 1 and S1−S6 (Supporting Information). Crystals of **12** were grown by slowly cooling a $CH_2Cl_2$/pentane solution. Slowly

(13) Nolan, S. P.; Porchia, M.; Marks, T. J. *Organometallics* **1991**, *10*, 1450−1457.

(14) *TEXSAN-TEXRAY Structure Analysis Package*; Molecular Structure Corp.: 1985.

**Table 1.** Summary of Crystal Structure Data

| | | | |
|---|---|---|---|
| formula | $C_{26}H_{42}ZrI_2$ (**12**) | $C_{26}H_{42}HfI$ (**13**) | $C_{26}H_{42}ZrI$ (**14**) |
| *M* | 699.65 | 660.01 | 572.74 |
| crystal size (mm) | 0.27 × 0.18 × 0.15 | 0.45 × 0.29 × 0.20 | 0.52 × 0.22 × 0.14 |
| crystal system | orthorombic | monoclinic | monoclinic |
| space group | *Pccn* | $P2_1/c$ | $P2_1/c$ |
| *a* (Å) | 10.366(3) | 12.820(4) | 12.835(3) |
| *b* (Å) | 31.172(7) | 12.860(4) | 12.917(2) |
| *c* (Å) | 17.099(3) | 16.833(4) | 16.861(5) |
| $\beta$ (deg) | na | 109.40(2) | 109.38(2) |
| *V* (Å$^3$) | 5525(4) | 2618(2) | 2637(2) |
| *Z* | 8 | 4 | 4 |
| $r_{calc}$ | 1.682 | 1.675 | 1.442 |
| $m$(Mo $K_\alpha$) (cm$^{-1}$) | 26.14 | 51.26 | 15.77 |
| radiation | graphite-monochromated Mo Kα $\lambda = 0.71069$ Å | | |
| temp, °C | −120 | −120 | −120 |
| scan type | $\omega - \theta$ | | |
| $2\theta$ range (deg) | 4.0−52.0 | 4.0−46.0 | 4.0−48.0 |
| scan width (deg) | 1.00−0.35 tan $\theta$ | | |
| unique data | 6050 | 3825 | 4348 |
| unique data $I > 3\sigma(I)$ | 3445 | 3120 | 3179 |
| no. of parameters | 431 | 254 | 422 |
| $R(F)$ | 0.032 | 0.032 | 0.023 |
| $R_w(F)$ | 0.032 | 0.039 | 0.030 |
| GOF | 1.12 | 1.88 | 1.35 |

cooling pentane solutions of **13** and **14** yielded crystals suitable for X-ray diffraction. A yellow prismatic crystal of **12**, an orange prismatic crystal of **13**, and an orange columnar crystal of **14** were selected for X-ray crystallographic study.

The intensities of three representative reflections for **12**, **13**, and **14** were measured every 90 min of X-ray exposure and showed no significant decay for each compound studied. The intensity data for each structure were corrected for Lorentz-polarization effects. Analytical absorption corrections were applied for **12** and **13**. An empirical absorption correction, using the program DIFABS,[15] was applied for **14**. The resulting transmission factors are 0.51−0.70 for **12**, 0.18−0.39 for **13**, and 0.96−1.05 for **14**. Corrections for secondary extinction were also applied. The secondary extinction coefficients for **12**, **13**, and **14** are respectively $1.1610 \times 10^{-6}$, $3.2600 \times 10^{-5}$, and $7.0611 \times 10^{-6}$. Heavy atoms for each structure were initially located by direct methods. The remaining atoms were located from Fourier difference maps. The final full-matrix least-squares refinement with anisotropic thermal parameters for all non-hydrogen atoms gave a final *R* of 0.032 ($R_w = 0.032$) for **12**, 0.032 ($R_w = 0.039$) for **13**, and 0.023 ($R_w = 0.030$) for **14**. All hydrogen atoms were located for **12** and **14** and were included in the final refinement with isotropic thermal parameters. Hydrogen atoms for **13** were placed at idealized positions and included in the final refinement. The largest peaks remaining in the difference maps for **12**, **13**, and **14** were respectively 0.75, 1.88, and 0.47 e$^-$/Å$^3$.

**Photoelectron Spectroscopic Studies of 7, 12, and 14.** High-resolution UV PE spectra were acquired as described elsewhere.[16] Resolution, measured on the He $1s^{-1}$ line, was always 25 meV. The spectra were recorded in the 145−190 °C temperature range, depending upon the particular complex. The spectral profiles remained constant over a ±30 °C temperature range, thus ruling out significant decomposition processes in the gas phase.

**Theoretical Methods.** Ab initio relativistic effective core potentials (RECPs) were employed in the molecular calculations using the restricted Hartree−Fock (RHF) formalism for the closed-shell states and the restricted open Hartree−Fock (ROHF) formalism for the open-shell states. The ionization energies of the lower lying ionic states of each symmetry were evaluated using the ΔSCF procedure, which accounts only for relaxation contributions to the total reorganization energy.[17] Single-point energy MP2 calculations were performed to account for correlation effects in calculating the dissociation energies. Core electrons of Zr and I atoms were replaced by the RECPs of Hay and Wadt.[18] Valence Gaussian bases were contracted in a double-ζ quality, and for iodine a "d" polarization function (α = 0.25) was added. The standard 6-31G basis sets of Pople et al.[19] were adopted for the C and H atoms. The geometries of the $Cp_2ZrI$, $Cp_2ZrI_2$, $Cp^{tt}_2ZrI$, and $Cp^{tt}_2ZrI_2$ complexes were optimized using gradient techniques. All calculations were performed using the HONDO-95.3 program[20] on an IBM SP system. Van der Waals interaction energies were evaluated using molecular mechanics MM+ calculations.[21]

## Results

**Synthetic Procedures.** The syntheses of $Cp_2^{tt}TiCl$ (**4**), $Cp^{tt}_2ZrCl_2$ (**7**), and $Cp^{tt}_2HfCl_2$ (**8**), precursors to the present metallocenes, are either new or represent crucial refinements to earlier procedures.[9] Thus, the direct synthesis of **4** from $TiCl_3$ (eq 4) affords considerable improvement in yield over the

$$TiCl_3 + 2NaCp^{tt} \xrightarrow{THF} \underset{\mathbf{4}}{Cp_2{}^{tt}TiCl} \qquad (4)$$

previous,[9a] multistep synthesis, involving reduction of $Cp^{tt}_2TiCl_2$, prepared in turn via a low-yield route. The $MCl_4 + 2NaCp^{tt}$ routes to **7** and **8** reported here are refinements of earlier procedures;[9b] both achieve facile and rapid isolation of products. The substantially differential solubilities of **7** and **8** (low at room temperature in pentane, diethyl ether, toluene, and methylene chloride; appreciable in hot toluene and $CH_2Cl_2$; and good in THF at room temperature) allow a clean and quantitative separation from byproduct NaCl by THF extraction. Moreover, a slight stoichiometric excess of $NaCp^{tt}$ is used to avoid side reactions to mono-$Cp^{tt}$-substituted intermediates. Unreacted $NaCp^{tt}$, also soluble in THF, is conveniently converted to soluble neutral organic products by reaction with $CH_2Cl_2$. Thus, either a mixture of $CH_2Cl_2$ and THF or pure THF can be used to extract **7** and **8**, which, once separated from inorganic solids, can be easily washed with pentane to remove organic impurities.

The preparation of group 4 metallocene iodides with bulky $Cp^{tt}$ ancillary ligands is significantly more difficult than for less hindered metallocenes. Unlike the halide metathetical synthesis of $(Me_5C_5)_2TiI$ from the chloride homologue,[12] the preparation of $Cp^{tt}_2TiI$ (**5**) requires a larger (10-fold) LiI excess which, however, partially decomposes the product, thus reducing the yield. The diiodide compounds **11** and **12** can be more efficiently prepared by reaction of the corresponding, readily prepared metallocene dimethyl complexes (**9** and **10**) with $I_2$ (eq 5). The

$$\underset{\mathbf{9},\ M = Hf}{\underset{\mathbf{10},\ M = Zr}{Cp_2{}^{tt}MMe_2}} + 2I_2 \xrightarrow{toluene} \underset{\mathbf{12},\ M = Zr}{\underset{\mathbf{11},\ M = Hf}{Cp_2{}^{tt}MI_2}} + 2MeI \qquad (5)$$

synthesis of **9** and **10** proceeds cleanly from **7** and **8**, respectively, using the indicated (see Experimental Section for details) methylation conditions ($Cp_2^{tt}MCl_2 + 2MeLi$). No significant differences in reactivity of complexes **7** and **8** with MeLi are observed. The route to lower valent Zr(III) and Hf(III) iodide complexes is a modification of the literature procedure[9] and involves reduction of **11** and **12** with K/Hg amalgam in THF (eq 6). The reaction proceeds cleanly under these condi-

(15) Walker, N.; Stuart, D. *Acta Crystallogr*. **1983**, *A39*, 158−166.
(16) Gulino, A.; Ciliberto, E.; Di Bella, S.; Fragalà, I.; Seyam, A. M.; Marks, T. J. *Organometallics* **1992**, *11*, 3248.
(17) Di Bella, S.; Gulino, A.; Lanza, G.; Fragalà, I.; Marks, T. J. *J. Phys. Chem.* **1993**, *97*, 11673.
(18) Hay, P. J.; Wadt, W. R. *J. Chem. Phys.* **1985**, *82*, 299.
(19) Hehre, W. J.; Ditchfield, R.; Pople, J. A. *J. Chem. Phys.* **1972**, *56*, 2257.
(20) Dupuis, M.; Marquez, A.; Davidson, E. R. *HONDO 95.3 from CHEM-Station*; IBM Corp.: Kingston, NY, 1995.
(21) *HyperCube HYPERCHEM*, Release 4.5 for Windows; HyperCube: 1995.

$$\underset{\textbf{11}, M = Hf}{Cp^{tt}_2MI_2} + K/Hg \xrightarrow{THF} \underset{\textbf{13}, M = Hf}{Cp^{tt}_2MI} \quad (6)$$
$$\textbf{12}, M = Zr \qquad \textbf{14}, M = Zr$$

tions. However, the reduction of **12** does not proceed to completion under the same conditions as for **7** (see Experimental Section for details).

**$^1$H NMR Titration Studies for Calorimetry.** Calorimetric measurement reactions were first validated by $^1$H NMR titration studies, and eqs 7 and 8 were found suitable for reliable thermochemistry. Products **6**, **11**, and **12** were identified by

$$Cp^{tt}_2MI + 1/2I_2 \xrightarrow{\text{toluene}} Cp^{tt}_2MI_2 \qquad M = Ti, Zr, Hf \quad (7)$$

$$Cp^{tt}_2MMe_2 + 2I_2 \xrightarrow{\text{toluene}} Cp^{tt}_2MI_2 + 2MeI \qquad M = Zr, Hf \quad (8)$$

comparison to $^1$H NMR spectra of authentic samples and yielded appropriate integration with respect to an internal adamantane standard. No evidence for hindered Cp ring or *tert*-butyl group rotation at room temperature is observed in the NMR of these compounds. $(Me_5C_5)_2TiI_2$ was identified by comparison with literature $^1$H NMR data.[22]

**Molecular Structure Studies.** The crystal structure of $Cp^{tt}_2ZrI_2$ (**12**) consists (Figure 1) of unassociated monomers, consistent with the structures of the related titanocene $Cp^{tt}_2TiCl_2$[9a] and $[(SiMe_3)_2C_5H_3]_2ZrX_2$ (X = F, Br, I).[23] Selected bond lengths and angles are presented in Tables 2 and 3, respectively.[24] The Zr ligation is, not unexpectedly, pseudotetrahedral, and the ring *tert*-butyl groups "straddle" the Zr−I bonds to minimize steric interactions (Figure 1). The Zr−I bond lengths (2.8454(8) and 2.8258(8) Å) are in reasonable agreement with those in $Cp_2ZrI_2$ (2.832(8) Å)[25] and $[(Me_3Si)_2C_5H_3]_2ZrI_2$ (2.828(8) Å)[23] (Table 4). The I−Zr−I bond angle is 97.10(2)°, only marginally larger than that in $Cp_2ZrI_2$ 96.2(1)° but considerably larger than those in various $Cp_2TiX_n$ complexes (∼93°, Table 4), and can be understood in terms of increased interligand steric repulsive effects (see below).

The Zr−Cp$^{tt}$ ring−centroid distances (2.250 Å av) in **12** are distinctly different from those reported in the ring-unsubstituted homologue (2.19 Å).[25] Similarly, the average Zr−C(Cp) distance is 2.550(6) Å in $Cp^{tt}_2ZrI_2$, compared to 2.48 Å in $Cp_2ZrI_2$.[23] The $Cp_{centr}$−Zr−$Cp_{centr}$ angle is significantly larger (133.0°) than that in $Cp_2ZrI_2$ (126.3°).[25] $Cp^{tt}_2ZrI_2$ shows close similarities to $[(Me_3Si)_2C_5H_3]_2ZrI_2$ in terms of metrical parameters (Table 4). The *tert*-butyl groups on both Cp$^{tt}$ rings of **12** are positioned toward the sterically least congested region of the molecule—at the front of the metallocene "clam shell". The ring methyl groups exhibit several close nonbonding interactions with the iodine ligands (Table 5), which are less than the sum of the methyl and iodine van der Waals radii (3.95−4.12 Å).[26] As mentioned above, seven nonbonded contacts involving the *tert*-butyl methyl groups are below this range, and such nonbonding interactions likely contribute to the unusually long Cp$^{tt}$−Zr bond lengths. This observation is in agreement with crystal structure data[9a] for sterically less congested $Cp^{tt}_2TiCl_2$, the ring methyl groups of which have close contacts with the Cl ligands. These range from 3.432 to 3.754 Å, substantially below the range calculated for the van der Waals radii sum for Cl and Me, 3.70−3.90 Å.[26] In view of the larger size of iodine, it

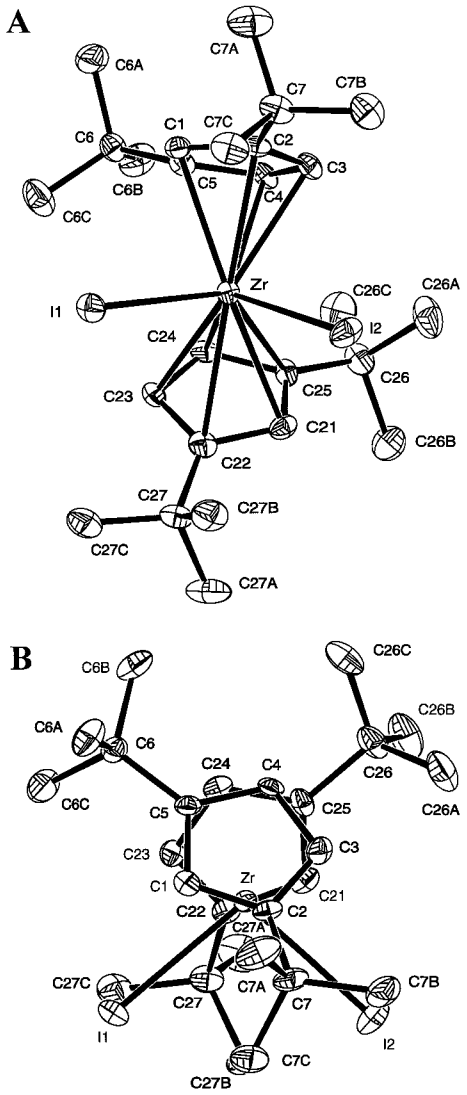


**Figure 1.** (A) ORTEP view of the molecular structure of $Cp^{tt}_2ZrI_2$ (**12**). (B) ORTEP view of the Cp$^{tt}$ conformations in $Cp^{tt}_2ZrI_2$. Thermal ellipsoids drawn at 50% probability level.

**Table 2.** Selected Intramolecular Bond Distances in $Cp^{tt}_2ZrI_2$ (**12**)

| atom | atom | distance Å | atom | atom | distance Å |
|---|---|---|---|---|---|
| I1 | Zr | 2.8454(8) | Zr | C21 | 2.575(6) |
| I2 | Zr | 2.8258(8) | Zr | C22 | 2.626(6) |
| Zr | C1 | 2.580(6) | Zr | C23 | 2.500(6) |
| Zr | C2 | 2.618(6) | Zr | C24 | 2.471(6) |
| Zr | C3 | 2.512(6) | Zr | C25 | 2.573(6) |
| Zr | C4 | 2.486(5) | Zr | Cent1[a] | 2.251 |
| Zr | C5 | 2.557(6) | Zr | Cent2[b] | 2.248 |

[a] Cent1 = Cp centroid for C1−C5. [b] Cent2 = Cp centroid for C21−C25.

**Table 3.** Selected Intramolecular Bond Angles in $Cp^{tt}_2ZrI_2$ (**12**)

| atom | atom | atom | angle (deg) |
|---|---|---|---|
| I1 | Zr | I2 | 97.10(2) |
| Cent1[a] | Zr | Cent2[b] | 133.0 |

[a] Cent1 = Cp centroid for C1−C5. [b] Cent2 = Cp centroid for C21−C25.

(22) Bruce, M. R. M.; Sclafani, A.; Tyler, D. *Inorg. Chem.* **1986**, *25*, 2546−2549.
(23) Antinolo, A.; Lappert, M. F.; Shing, A.; Winterborn, D. J. W.; Carty, A. J.; Taylor, N. J. *J. Chem. Soc., Dalton Trans.* **1987**, 1463−1471.
(24) A full listing of metrical parameters is given in the Supporting Information.
(25) (a) Bush M. A.; Sim, G. A. *J. Chem. Soc. A* **1971**, 2225−2229. (b) Prout, K.; Cameron, T. S.; Forder, R. A.; Critchley, S. R.; Denton, B.; Rees, G. V. *Acta Crystallogr.* **1974**, *B30*, 2290−2304.
(26) Huhee, J. E. *Inorganic Chemistry, Principles of Structure and Reactivity*, 3rd ed; Harper and Row: New York, 1983; pp 256−262.

**Table 4.** Comparison of Selected Metallocene Bond Lengths and Angles for Group 4 Metallocenes

| complex | M−X (Å) | M−C(Cp) average (Å) | M−Cp (Cent) average Å | X−M−X (deg) | Cent−M−Cent (deg) | ref |
|---|---|---|---|---|---|---|
| $Cp^{tt}_2ZrI_2$ (**12**) | (I1) 2.8454(8) (I2) 2.8258(8) | 2.550(6) | 2.250 | 97.10(2) | 133.0 | this work |
| $Cp_2ZrI_2$ | 2.832(8) | 2.48 | 2.19 | 96.2(1) | 126.3 | 25 |
| $[(Me_3Si)_2C_5H_3]_2ZrI_2$ | 2.828(8) (average) | 2.54 | 2.23 | 100.37(4) | 131.8 | 23 |
| $Cp^{tt}_2TiCl_2$ | 2.349(1) | 2.44 | 2.124 | 93.1(5) | 121.0 | 9a |
| $Cp_2TiCl_2$ | 2.364(2) (average) | 2.370(9) | 2.059 | 94.5(1) | 131.0 | *a* |
| $(MeC_5H_4)_2TiCl_2$ | 2.360(3) (average) | 2.31 | 2.067 | 93.15(8) | 130.2 | *b* |
| $(MeC_5H_4)_2TiCl_2$ | 2.344(2) | 2.42 | 2.11 | 94.2(1) | 133.4 | 38 |
| $(Me_5C_5)_2TiCl_2$ | 2.349(6) (average) | 2.44 | 2.128 | 92.94(4) | 137.4 | *c* |
| $Cp^{tt}_2HfI$ (**13**) | 2.7890(8) | 2.473(6) | 2.160 | | 134.0 | this work |
| $Cp^{tt}_2ZrI$ (**14**) | 2.8270(7) | 2.500(3) | 2.192 | | 133.3 | this work |
| $Cp^{tt}_2ZrCl$ | 2.423(1) | 2.50 | 2.200 | | 131.4 | 9b |
| $Cp^{tt}_2TiCl$ (**4**) | 2.337(1) | 2.39 | 2.066 | | 134.8 | 9a |
| $(Me_5C_5)_2TiCl$ | 2.363(1) | 2.388 | 2.06 | | 143.6 | 12 |
| $(Me_4C_5H)_2TiCl$ | 2.317(4) | 2.350 | 2.03 | | 139.1 | 38 |
| $(Me_4C_5H)_2TiI$ | 2.759(2) | 2.38(1) | 2.06 | | 139.3 | 38 |

[a] Clearfield, A.; Warner, D. K.; Soldarriaga, C. H.; Ropal-Molina, R.; Bernal, I. *Can. J. Chem.* **1975**, *53*, 1622. [b] Petersen, J. L.; Dahl, L. F. *J. Am. Chem. Soc.* **1975**, *97*, 6422. [c] McKenzie, T. C.; Sonner, R. D.; Bercaw, J. E. *J. Organomet. Chem.* **1975**, *102*, 457.

**Table 5.** Selected Close Intramolecular Nonbonded Contacts in $Cp^{tt}_2ZrI_2$ (**12**)

| contact | distance (Å) | contact | distance (Å) |
|---|---|---|---|
| I1 ··· C6C | 4.022(8) | I2 ··· C7B | 3.751(8) |
| I1 ··· C7C | 3.882(8) | I2 ··· C7C | 3.885(8) |
| I1 ··· C27B | 3.989(8) | I2 ··· C26A | 4.276(8) |
| I1 ··· C27C | 3.837(8) | I2 ··· C27B | 3.800(8) |

therefore appears that greater nonbonded interactions are operative in $Cp^{tt}_2ZrI_2$.

Crystals of $Cp^{tt}_2ZrI$ (**14**) are composed of unassociated monomers (Figure 2). Selected bond lengths and angles are presented in Tables 6 and 7, respectively.[24] The results are similar to those reported for related $Cp^{tt}_2ZrCl$.[9b] In contrast, the crystal structures of other Zr(III) metallocene halides, $(Cp_2ZrI)_2$[27] and $([(SiMe_3)_2C_5H_3]_2ZrCl)_2$,[28] consist of dimers in the solid state. Note that the slight change from $Cp(SiMe_3)_2$ to $Cp^{tt}$ ligation provides sufficient steric congestion to force the typically dimeric Zr(III) metallocenes to be monomeric. The ligation geometry about Zr in **14** is pseudotrigonal, and the $Cp^{tt}$ groups are disposed such that the complex possesses $C_2$ symmetry. The *tert*-butyl groups on both rings are again positioned toward the sterically least congested region and minimize steric interactions by "straddling" the Zr−I bond. In contrast to **12**, the *tert*-butyl groups are nearly eclipsed, presumably because of reduced repulsive interactions with the iodine ligand.

The Zr−I bond length in **14** (2.8270(7) Å) is slightly shorter than the average Zr−I distance in tetravalent **12** (2.835(8) Å). A slight shortening is similarly observed for the Ti−Cl bond in $Cp^{tt}_2TiCl$ (**4**) versus $Cp^{tt}_2TiCl_2$.[9a] The $Cp^{tt}$ centroid−Zr distance in **14** (2.192 Å) is similar to that in $Cp^{tt}_2ZrCl$ (2.200 Å)[9b] and shorter than that in **12** (2.250 Å), while significant shortening is observed in $Cp^{tt}_2TiCl$ versus $Cp^{tt}_2TiCl_2$ (Table 4). The average Zr−C(Cp) distance of 2.500(3) Å in **14** is significantly shorter than that in **12** (2.550(6) Å). Only two close nonbonding contacts are apparent in **14** (Table 8) versus seven in **12**, so **14** clearly possesses fewer repulsive nonbonded interactions than does **12**.

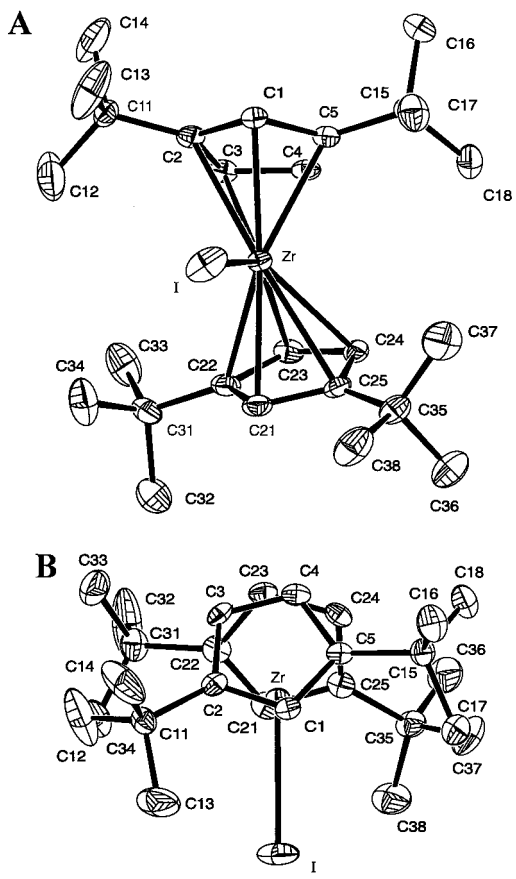


**Figure 2.** (A) ORTEP view of the molecular structure of $Cp^{tt}_2ZrI$ (**14**). (B) ORTEP view of the $Cp^{tt}$ conformations in $Cp^{tt}_2ZrI$. Thermal ellipsoids drawn at 50% probability level.

The molecular structure $Cp^{tt}_2HfI$ (**13**) is, to our knowledge, the first reported for a Hf(III) metallocene. It is isomorphous with $Cp^{tt}_2ZrI$ (**14**). A labeled ORTEP diagram is presented in Figure 3, while selected metrical parameters are presented in Tables 9 and 10.[24] The differences in metal−ligand bond lengths between **13** and **14** reflect the smaller $Hf^{IV}$ vs $Zr^{IV}$ ionic radius.[29] Thus, the Hf−I bond length in **13** (2.7890(8) Å) is 0.04 Å shorter than the Zr−I bond length in **14**. The average Hf−

(27) Wielstra, Y.; Gambarotta, S.; Meetsma, A.; de Boer, J. L.; *Organometallics* **1989**, *8*, 250−251.

(28) Hitchcock, P. B.; Lappert, M. F.; Lawless, G. A.; Oliver, H.; Ryan, E. J. *J. Chem. Soc., Chem. Commun.* **1992**, 474−476.

**Table 6.** Selected Intramolecular Bond Distances in $Cp^{tt}_2ZrI$ (**14**)

| atom | atom | distance Å | atom | atom | distance Å |
|---|---|---|---|---|---|
| I | Zr | 2.8270(7) | Zr | C22 | 2.496(3) |
| Zr | C1 | 2.504(3) | Zr | C23 | 2.462(3) |
| Zr | C2 | 2.554(3) | Zr | C24 | 2.487(3) |
| Zr | C3 | 2.478(3) | Zr | C25 | 2.567(3) |
| Zr | C4 | 2.456(3) | Zr | Cent1[a] | 2.186 |
| Zr | C5 | 2.485(3) | Zr | Cent2[b] | 2.189 |
| Zr | C21 | 2.514(3) | | | |

[a] Cent1 = Cp centroid for C1−C5. [b] Cent2 = Cp centroid for C21−C25.

**Table 7.** Selected Intramolecular Bond Angles in $Cp^{tt}_2ZrI$ (**14**)

| atom | atom | atom | angle |
|---|---|---|---|
| Cent1[a] | Zr | Cent2[b] | 134.0 |

[a] Cent1 = Cp centroid for C1−C5. [b] Cent2 = Cp centroid for C21−C25.

**Table 8.** Selected Intermolecular Nonbonded Interactions in $Cp^{tt}_2ZrI$ (**14**)

| contact | length (Å) |
|---|---|
| I ··· C13 | 3.995(6) |
| I ··· C37 | 4.335(6) |
| I ··· C38 | 4.035(5) |

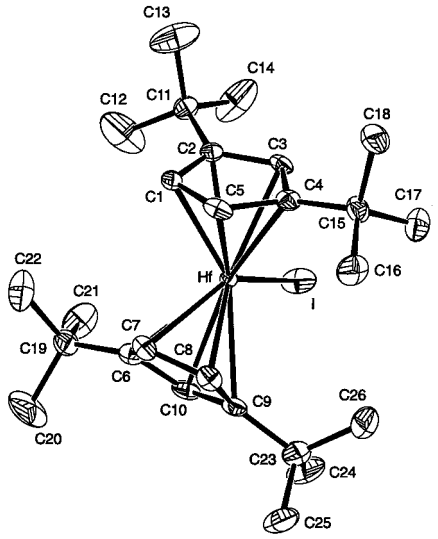


**Figure 3.** ORTEP view of the molecular structure of $Cp^{tt}_2HfI$ (**13**). Thermal ellipsoids drawn at 50% probability level.

**Table 9.** Selected Intramolecular Bond Distances for $Cp^{tt}_2HfI$ (**13**)

| atom | atom | distance Å | atom | atom | distance Å |
|---|---|---|---|---|---|
| Hf | I | 2.7890(8) | Hf | C7 | 2.425(6) |
| Hf | C1 | 2.461(6) | Hf | C8 | 2.460(6) |
| Hf | C2 | 2.529(6) | Hf | C9 | 2.538(6) |
| Hf | C3 | 2.496(6) | Hf | C10 | 2.498(6) |
| Hf | C4 | 2.455(6) | Hf | Cent1[a] | 2.160 |
| Hf | C5 | 2.432(6) | Hf | Cent2[b] | 2.161 |
| Hf | C6 | 2.445(6) | | | |

[a] Cent2 = Cp centroid for C1−C5. [b] Cent2 = Cp centroid for C6−C10.

C($Cp^{tt}$) bond length (2.473(6) Å) and the $Cp^{tt}$ centroid−Hf distance (2.160 Å), are both ∼0.03 Å shorter than the analogous distances in **14**. Given the absence of structural differences between **13** and **14**, it is reasonable to expect similar nonbonded interactions.

**Table 10.** Selected Intramolecular Bond Angles in $Cp^{tt}_2HfI$ (**13**)

| atom | atom | atom | angle (deg) |
|---|---|---|---|
| Cent1[a] | Hf | Cent2[b] | 134.6 |

[a] Cent2 = Cp centroid for C1−C5. [b] Cent2 = Cp centroid for C6−C10.

**Table 11.** Enthalpies of Metallocene Iodination Per Mole of Complex in Toluene and Derived Metal−Ligand Bond Enthalpies

| compound | reaction (eq) | $\Delta H_{rxn}$ (kcal/mol complex) | $D(L_nM-R)$ (kcal/mol) |
|---|---|---|---|
| $Cp^{tt}_2TiI$ (**5**) | 4 | −22.8(5) | $D[(L_nTi(I)-I)] = 40.6(5)$ |
| $(Me_5C_5)_2TiI$ (**2**) | 4 | −34.5(6) | $D[(L_nTi(I)-I)] = 52.3(6)$ |
| $Cp^{tt}_2ZrI$ (**14**) | 4 | −40.2(5) | $D[(L_nZr(I)-I)] = 58.0(5)$ |
| $Cp^{tt}_2HfI$ (**13**) | 4 | −43.4(4) | $D[(L_nHf(I)-I)] = 61.2(4)$ |
| $Cp^{tt}_2ZrMe_2$ (**10**) | 5 | −73.1(6) | $D[(L_nZr\text{-}Me_2)] = 43(1)$ |
| $Cp^{tt}_2HfMe_2$ (**9**) | 5 | −70.5(3) | $D[(L_nHf\text{-}Me_2)] = 47.6(9)$ |
| $TiI_4$ | | | $D(I_3Ti-I) = 56(2)$[a] |
| $ZrI_4$ | | | $D(I_3Zr-I) = 59(2)$[a] |

[a] From ref 31.

**Thermochemical Measurements.** Reaction enthalpies and derived metal−halogen disruption enthalpies are presented in Table 11. All uncertainties for $\Delta H_{rxn}$ are reported to 95% confidence limits, while those of $D(L_nM-R)$ bonds include both experimental and literature auxiliary value uncertainties. D(I−I)[30] and D(Me−I)[30] were taken from the indicated references. Note that $D[Cp^{tt}_2Ti(I)-I]$ is significantly weaker than $D[(Me_5C_5)_2Ti(I)-I]$, by 11.7 kcal/mol, probably due to the greater steric encumberance, and that $D[(Me_5C_5)_2Ti(I)-I]$ compares favorably with $D(I_3Ti-I) = 56(2)$ kcal/mol.[31] Turning to the Zr homologue, note that the presently measured value for $D[Cp^{tt}_2Zr(I)-I]$ (58.0(5) kcal/mol; Table 11) closely agrees with $D(I_3Zr-I) = 59$ kcal/mol calculated from the estimated enthalpies of formation of $ZrI_3(g)$[31b] and $ZrI_4(g)$,[31b] which is probably somewhat less reliable than $D(I_3Ti-I)$. [31b]

**Electronic Structures of $Cp_2ZrX_n$ Complexes.** Optimized HF metrical parameters for the present complexes agree well with the experimental data from the diffraction experiments (Table 12). The *tert*-butylcyclopentadienyl substituents lie in the sterically least congested regions of the molecules, as found in the crystal structures. The $Zr-Cp_{centr}$ and Zr−I bond lengths are slightly overestimated, possibly due to omission of electron correlation. Nevertheless, the curious contraction of the $Zr-Cp_{centr}$ bond length on passing from Zr(IV) to Zr(III) complexes is found, in agreement with X-ray data. Eigenvalues and population analysis for the $^2A_1$ ground-state of $Cp^{tt}_2ZrI$ are reported in Table 13. Clearly, the iodine ligation strongly perturbs the $Cp^{tt}_2Zr$ fragment and induces a substantial admixture of the interacting fragment MOs. The mixing is mainly restricted to orbitals of $a_1$ and $b_2$ representations under $C_{2v}$ symmetry, namely the 104a, 99a and 100a, 98a pairs, and represents the consequence of two-orbital, four-electron interactions. The partially filled 105a ($d_{x^2-y^2}$) orbital, responsible for the metal $d^1$ configuration, remains essentially nonbonding in character and represents the HOMO. The contour plot analysis

(29) (a) Weast, R. C., Ed. *Handbook of Chemistry and Physics*, 62nd ed; CRC Press: Boca Raton, FL, 1984. (b) Shannon, R. D. *Acta Crystallogr.* **1976**, *A32*, 751−767.

(30) (a) Griller, D.; Kanabus-Kaminska, J. J.; Maccoll, A. *J. Mol. Struct.* **1988**, *163*, 125−131. (b) McMillan, D. F.; Golden, D. M. *Annu. Rev. Phys. Chem.* **1982,** *33*, 493−532. (c) Reference 29a, pp F171−F190 and references therein. (d) Benson, S. W. *Thermochemical Kinetics*, 2nd ed.; John Wiley and Sons: New York, 1976; p 309.

(31) (a) Calculated from gas-phase heats of formation of $TiI_4$ found in ref 31b and the gas-phase heat of formation of $TiI_3$ found in ref 31c. (b) Chase, M. W.; Davies, C. A.; Downey, J. R. Jr.; Feurir, D. J.; McDonald, R. A.; Syverund, A. N. *J. Phys. Chem. Ref. Data* **1985**, *14*, Suppl. 1. (c) Girichev, G. V.; Lapshina, S. B.; Giricheva, N. I. *Russ. J. Phys. Chem.* **1992**, *66*, 557−579.

**Table 12.** Selected Optimized Bond Lengths (Å) and Angles (deg)[a] in Zirconocene Iodides

| | $Cp^{tt}_2ZrI_2$ | $Cp^{tt}_2ZrI$ | $Cp_2ZrI_2$[b] | $Cp_2ZrI$ |
|---|---|---|---|---|
| Zr−I | 2.939 (2.836) | 2.976 (2.827) | 2.909 (2.832) | 2.928 |
| $Zr-C(Cp)_{average}$ | 2.624 (2.550) | 2.584 (2.500) | 2.587 (2.48) | 2.605 |
| $Zr-Cp_{centr}$ | 2.331 (2.25) | 2.284 (2.192) | 2.261 (2.19) | 2.307 |
| $C(Cp)-C(Cp)_{average}$ | 1.419 (1.422) | 1.419 (1.414) | 1.414 (1.42) | 1.415 |
| $C(Cp)-C(t\text{-}Bu)_{average}$ | 1.532 (1.528) | 1.533 (1.523) | | |
| $Cp_{centr}-Zr-Cp_{centr}$ | 132.1 (133.0) | 131.9 (133.3) | 131.5 (126.3) | 132.7 |
| I−Zr−I | 97.7 (97.1) | | 98.7 (96.2) | |

[a] Values in parentheses refer to experimental data. [b] Data from ref 25.

**Table 13.** Ab Initio Orbitals, Eigenvalues, and Population Analysis for $Cp^{tt}_2ZrI$

| | | | | Zr | | | | | | |
|---|---|---|---|---|---|---|---|---|---|---|
| MO | GS (−eV) | ΔSCF (eV) | IE[a] (eV) | 5s | 5p | 4d | I | $2C_5H_3$ | $4C(CH_3)_3$ | dominant character |
| 105a | 7.81 | 5.75 | 5.72 (**x**) | 6 | 0 | 87 | 1 | 6 | 0 | $d_{x^2}$ |
| 104a | 8.10 | 7.36 | 7.54 (**a**) | 0 | 0 | 3 | 53 | 42 | 2 | $I_{5p} + \pi_2$ |
| 103a | 8.56 | 7.90 | 7.98 (**b′**) | 0 | 2 | 5 | 3 | 82 | 8 | $\pi_2 + d_{xz}$ |
| 102a | 8.87 | 7.60 | 7.54 (**a**) | 0 | 1 | 7 | 89 | 2 | 1 | $I_{5p} + d_{xz}$ |
| 101a | 9.14 | 8.40 | 8.30 (**b″**) | 0 | 1 | 15 | 2 | 73 | 9 | $\pi_2 + d_{xy}$ |
| 100a | 9.56 | | 8.60 (**b‴**) | 1 | 6 | 1 | 37 | 54 | 1 | $\pi_2 + \sigma$ Zr−I |
| 99a | 9.76 | | | 0 | 0 | 16 | 38 | 43 | 3 | $\pi_2 + I_{5p} + d_{yz}$ |
| 98a | 9.92 | | 9.44 (**c**) | 1 | 1 | 19 | 44 | 33 | 2 | $\sigma$ Zr−I + $\pi_2 + d_{z^2}$ |

[a] Experimental data, see Figure 5.

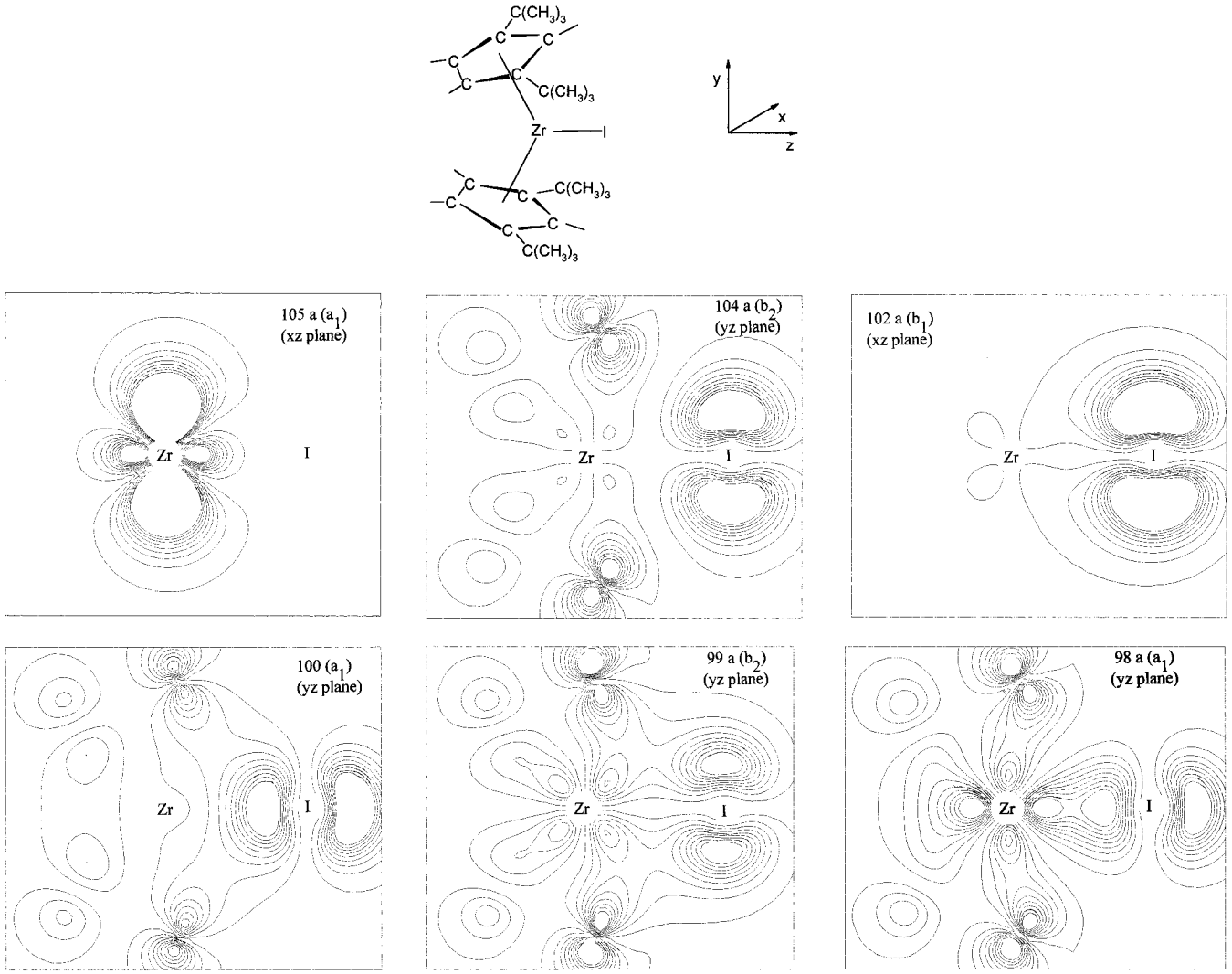


**Figure 4.** Electron density contour plots of significant MOs of $Cp^{tt}_2ZrI$. The contour value is 0.002 $e^-/Å^3$.

of the relevant $Cp^{tt}_2ZrI$ MOs provides evidence (Figure 4) of Zr−I $\sigma$ bonding in the 98a and 100a MOs as well as of considerable Zr−I $\pi$ bonding in MOs 104a and 99a. Note that the nodal properties of the 100a and 104a MOs provide clear evidence of the aforementioned nonbonded interligand repulsive effects.

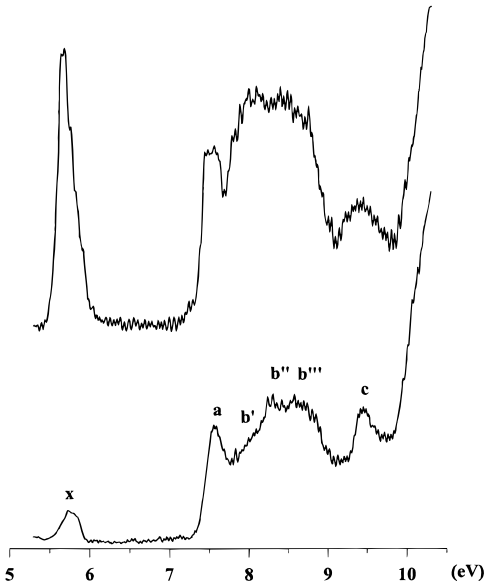


**Figure 5.** Gas-phase He I (bottom) and He II (top) PE spectra of $Cp^{tt}_2ZrI$ (5−10.5 eV).

**Table 14.** Gas-Phase PE Data for Selected $Cp_2ZrI_n$ (A) and $Cp_2ZrCl_2$ (B) Complexes

(A) $Cp_2ZrI_n$

| $Cp_2ZrI_2$[a] | $Cp^{tt}_2ZrI_2$ | $Cp^{tt}_2ZrI$ | assignment |
|---|---|---|---|
| | | 5.72 (**x**) | Zr ($d_{x^2-y^2}$) |
| 8.10 (**a**) | 7.48 (**a**) | | |
| 8.40 (**b**) | 7.69 (**b**) | 7.54 (**a**) | $I_{5p}$ |
| 9.50 (**c**) | 8.00 (**c**) | | |
| | 8.72 (**d**) | 7.98 (**b′**) | |
| 10.00 (**d**) | 9.03 (**e**) | 8.30 (**b″**) | $\pi_2$-Cp |
| | 9.37 (**f**) | 8.60 (**b‴**) | |
| | 9.90 (**g**) | 9.44 (**c**) | $\sigma$ Zr−I |

(B) $Cp_2ZrCl_2$

| $Cp_2ZrCl_2$[a,b] | $Cp'_2ZrCl_2$[b] | $Cp^{tt}_2ZrCl_2$ | assignment |
|---|---|---|---|
| 8.60 (**a**) | 7.55 (**a**) | 7.84 (**a**) | |
| 9.08 (**b**) | 7.97 (**a′**) | 8.30 (**b**) | $\pi_2$-Cp |
| 9.84 (**c**) | | 8.95 (**c**) | |
| 10.45 (**d**) | 9.96 (**b**) | 10.43 (**d**) | |
| 11.12 (**e**) | 10.85 (**c**) | | |
| | 11.06 (**c′**) | 11.07 (**e**) | $Cl_{3p}$ |
| 11.33 (**f**) | 11.52 (**d**) | | |
| 13.10 (**g**) | 12.40 (**e**) | 12.31 (**f**) | |

[a] Reference 32. [b] Reference 34.

The PE spectra of $Cp^{tt}_2ZrI$ are shown in Figure 5, and relevant PE data are collected in Table 14A. The lower IE region (5.50−10.00 eV) consists of four resolved features, **x**, **a**, **b**, and **c**. In the broad and overlapped band envelope **b**, three IE values can be distinguished at 7.98 (**b′**), 8.30 (**b″**), and 8.60 (**b‴**) eV. Under higher energy He II radiation, band **x** increases dramatically in intensity relative to the other bands, while band **d** and, to some extent, band **a** become less intense. It is well known[32−34] that, in a simple LCAO-MO formulation, $I_{5p}$- and metal 4d-based MOs respond distinctively to the energy of the ionizing source since they have considerably smaller or greater[32−34] cross-sections, respectively, relative to $C_{2p}$ (hence Cp-$\pi_2$)-based MOs. Therefore, PE intensity changes on varying the photon energy are highly diagnostic and argue for assignment of band **x** to ionization from the 105a MO, almost totally metal 4d in character and responsible for the open-shell $4d^1$ Zr(III) configuration. In accordance with the ΔSCF ab initio calculations, band **a** can be assigned to the 104a and 103a MOs, both having a dominant $I_{5p}$ contribution. Similarly, band **c** is assigned to the 98a MO, formally representing the Zr−I $\sigma$ bond. Finally, features **b** can be assigned to Cp-$\pi_2$ MOs (Table 14A).

Ground-state ab initio population data for $Cp^{tt}_2ZrI_2$ are compiled in Table 15. While the MOs formally representing the Zr−I $\sigma$ bonds (100a and 101a) can be easily identified, among the remainder there is not a clear-cut discrimination between I- and Cp-based MOs due to substantial $I_{5p}(\pi)$ and Cp-$\pi_2$ admixture. Nevertheless, there is a strict correlation between their energy grouping and the dominant atomic character. Thus, MOs in the 8.13−8.48 eV range represent $I_{5p}(\pi)$ orbitals, while those in the 9.38−9.94 eV interval are predominantly Cp-$\pi_2$ in character. The features of the photoelectron spectra (Figure 6) as well as the related data are in good agreement with the computational findings, since three groups of bands, the IE values of which agree with the ΔSCF data (Table 15), can be detected in the spectra. Even more interesting is the evidence for a pronounced falloff in relative intensities of bands **a**−**c** and **g** upon switching to higher energy He II radiation. Based on the aforementioned diagnostic criteria,[32−34] bands **a**−**c** and **g** can be confidently associated with MOs closely identifiable with $I_{5p}$ lone pairs and with Zr−I $\sigma$ bonds, respectively. The sharp line shapes and narrow fwhms (0.30 eV) of bands **a**−**c** are indicative of essentially nonbonding character in the corresponding MOs. Moreover, the average energetic separation (∼0.25 eV), approximately one-half of the corresponding splitting observed in HI,[35] $CH_3I$,[35] and the linear triatomic $ZnI_2$,[36] is also in agreement with second-order spin−orbit coupling effects of the heavy iodine atoms.[32] This observation argues for extensive $\pi-\pi$ mixing of $\pi$-type "lone pair" iodine orbitals with the metal fragment Cp-$\pi_2$ orbitals and, in turn, provides a sensitive experimental probe of interligand mixing.[35] The remaining bands **d**, **e**, and **f** are associated with ionization of Cp-$\pi_2$-based MOs. Insufficient resolution in the He II spectra precludes quantitative evaluation of He I vs He II intensity variations. Nevertheless, there is qualitative evidence that band **d** exhibits reduced intensity in the He II spectrum, thus favoring the assignment to MO 104a, which has a greater $I_{5p}$ content (Table 15).

The He I spectrum of $Cp^{tt}_2ZrCl_2$ exhibits five bands in the 7.5−12-eV region (Table 14B; Figure S7, Supporting Information). Relative intensity changes on passing to He II radiation, as well as the close analogy of the present PE features to the previously reported PE spectral pattern of the $Cp_2ZrCl_2$ parent complex,[32] suggest analogous assignments (Table 14B).

Finally, we comment further concerning the effects of *tert*-butyl substitution upon PE spectral features in the present complexes. It has been observed[33] that polymethylation of Cp ligands in $Cp_2MX_2$ complexes brings about a generally lower IE shift of both Cp (∼0.25 eV per methyl group) and $X_{np}$ ionizations (∼0.2 eV). The effect is approximately additive within a given series, and the presently observed energy shift due to two *tert*-butyl groups per ring appears electronically comparable to that from approximately four methyl groups per ring.[33]

**Molecular Structure Trends.** The present theoretical as well as experimental PE data can be put in perspective by considering

(32) Cauletti, C.; Clark, J. P.; Green, J. C.; Jackson, S. E.; Fragalà, I. L.; Ciliberto, E.; Coleman, A. W. *J. Electron Spectrosc. Relat. Phenom.* **1980**, *18*, 61.
(33) Vondrak, T.; Mach, K.; Varga, V. *Organometallics* **1992**, *11*, 2030.
(34) Ciliberto, E.; Condorelli, G.; Fagan, P. J.; Manriquez, J. M.; Fragalà, I.; Marks, T. J. *J. Am. Chem. Soc.* **1981**, *103*, 4755.
(35) Brogli, F.; Heilbronner, E. *Helv. Chim. Acta* **1971**, *54*, 1423.
(36) Cocksey, B. G.; Eland, J. H. D.; Danby, C. J. *J. Chem. Soc., Faraday Trans. 2* **1973**, *69*, 1588.

**Table 15.** Ab Initio Orbitals, Eigenvalues, and Population Analysis for $Cp^{tt}_2ZrI_2$

| | | | | Zr | | | | | | |
|---|---|---|---|---|---|---|---|---|---|---|
| MO | GS (−eV) | ΔSCF (−eV) | IE[a] (eV) | 5s | 5p | 4d | 2I | $2C_5H_3$ | $4C(CH_3)_3$ | dominant character |
| 108a | 8.13 | 7.62 | 7.69 (**b**) | 0 | 0 | 4 | 42 | 47 | 6 | $I_{5p} + \pi_2 + d_{yz}$ |
| 107a | 8.41 | 7.51 | 7.48 (**a**) | 0 | 0 | 1 | 73 | 24 | 2 | $I_{5p} + \pi_2$ |
| 106a | 8.48 | 7.99 | 8.00 (**c**) | 0 | 0 | 4 | 70 | 24 | 3 | $I_{5p} + \pi_2 + d_{xy}$ |
| 105a | 9.38 | 8.72 | 9.03 (**e**) | 0 | 2 | 8 | 31 | 53 | 6 | $\pi_2 + I_{5p} + d_{xz}$ |
| 104a | 9.42 | | 8.72 (**d**) | 0 | 1 | 10 | 62 | 23 | 4 | $I_{5p} + \pi_2 + d_{x^2-y^2}$ |
| 103a | 9.89 | | 9.37 (**f**) | 0 | 2 | 16 | 25 | 47 | 10 | $\pi_2 + I_{5p} + d_{z^2} + d_{x^2-y^2}$ |
| 102a | 9.94 | | | 0 | 3 | 12 | 42 | 36 | 6 | $\pi_2 + I_{5p} + d_{yz}$ |
| 101a | 10.20 | | 9.90 (**g**) | 0 | 7 | 15 | 74 | 3 | 1 | $\sigma$ Zr−I + $d_{xz}$ |
| 100a | 10.30 | | | 4 | 6 | 7 | 79 | 3 | 1 | $\sigma$ Zr−I + $d_{z^2}$ |
| 99a | 10.69 | | | 0 | 0 | 24 | 20 | 51 | 5 | $\pi_2 + I_{5p} + d_{yz}$ |

[a] Experimental data, see Figure 6.

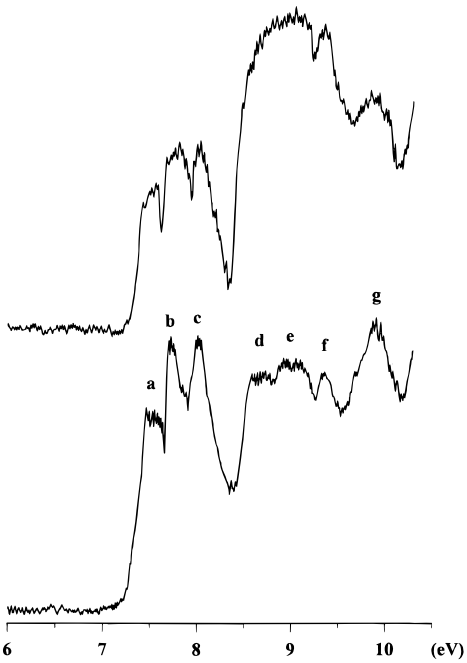


**Figure 6.** Gas-phase He I (bottom) and He II (top) PE spectra of $Cp^{tt}_2ZrI_2$ (5−10.5 eV).

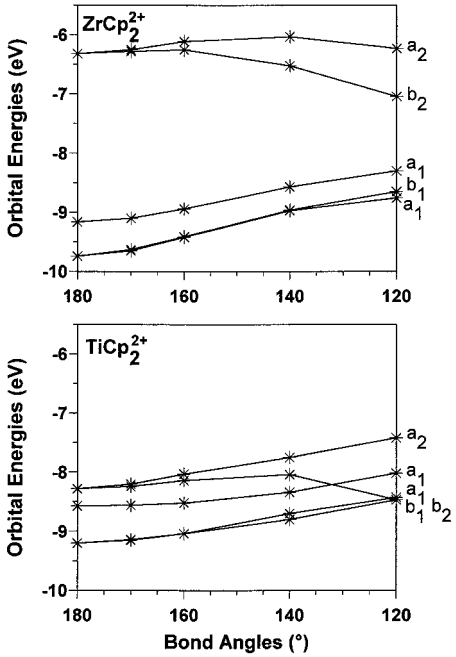


**Figure 7.** Energy dependence upon ring centroid−M−ring centroid bending of d-metal-based orbitals in the $Cp_2M$ fragment.

the large experimental structural database for $Cp_2MX_n$ molecules (Table 4). It is well known that coordination of $\sigma$ bonded ligands induces bending of the $Cp_2M$ fragment out of a ring-coplanar geometry and, in turn, profoundly affects bonding interactions within the fragment.[37] The leading Cp−M interactions (among the $e_{1g}$ Cp and metal $d_{xy,yz}$ orbitals) are modified to varying extents, while new interactions become operative due to the lower $C_{2v}$ symmetry. The net result is that orbitals $a_2$ and $b_2$, capable of $\pi$ bonding with the ancillary X ligand, are stabilized and more accessible in terms of orbital energy matching. Orbitals which extend either in the *xz* ($2a_1$, $b_1$) or *xy* ($1a_1$) planes lie higher in energy and, hence, are less favored for $\sigma$ M−X bonding (Figure 7). Therefore, the interplay between molecular structure and the nature of the ligand array mirrors competing $\sigma$ vs $\pi$ M−X bonding since strong $\sigma$-donor capabilities favor ring coplanarity while $\pi$-donation should force greater bending.

The present theoretical results demonstrate that iodine behaves as a strong $\sigma$ and $\pi$ donor ligand. Moreover, these capabilities are greatly enhanced upon ring alkyl substitution, as demonstrated by the lower lying ionization energies of $I_{5p}$-related MOs in $Cp^{tt}_2ZrI_2$ versus those in $Cp_2ZrI_2$ (Table 14). Similarly, IE data for a large series of polymethyl ring-substituted $Cp_2TiCl$ complexes show that $Cl_{3p}$ ionizations exhibit progressively lower energies upon ring methylation.[33] Nevertheless, I remains a better donor than Cl, as evidenced by the consistently lower absolute IE values (∼8 vs ∼10 eV). In this connection, note also that bending toward ring coplanarity considerably reduces nonbonded interligand repulsions, as evidenced by the less extensive I−Cp MO mixing as ∠Cp(centroid)−M−Cp(centroid) increases from $\theta$ = 126° to 133° in $Cp_2ZrI_2$ (Table S13, Supporting Information), the effect being considerably more pronounced in the ring *tert*-butyl-substituted analogue. Thus, the $\theta$ bending angle (126.3°) found in $Cp_2ZrI_2$ (Table 4) represents a compromise between interligand repulsion and $\sigma/\pi$ Zr−I bonding (Zr−I = 2.832 Å). The more planar geometry found in $Cp^{tt}_2ZrI_2$ ($\theta$ =133°) reflects more severe interligand nonbonded repulsions. The $\sigma$ bond is consequently enforced; however, $\pi$ interactions are diminished with possible lengthening of the Zr−I bond (2.836 Å average). Similar geometrical effects are found in $Cp^{tt}_2ZrI$ (Zr−I = 2.8270(7) Å, $\theta$ = 133°), with the shorter Zr−I distance (Table 4) mirroring diminished interligand repulsions and more favorable $\pi$ interactions with the $b_2$ ($d_{yz}$) fragment orbital.

In the titanium homologues, the $\sigma/\pi$ interplay is more complex due both to the different energetic ordering of $Cp_2Ti$ fragment orbitals (Figure 7) and to reduced Ti−Cp distances, which render interligand repulsive interactions more severe. Thus, geometries more closely approaching ring-coplanar are

(37) Lauher, J. W.; Hoffmann, R. *J. Am. Chem. Soc.* **1976**, *98*, 1729.

found (Table 4). In $(Me_4C_5H)_2TiCl$, the Ti−Cl distance (2.317(4) Å)[38] and $\theta$ (139.1°)[38] can be contrasted with 2.363(1) Å and $\theta$ =143.6° in $(Me_5C_5)_2TiCl$.[11] As expected, the decrease of $\pi$ bonding with $\theta$ = 143.6° accounts well for the longer Ti−Cl distance (Table 4). A similar trend is observed in the $Cp_2TiCl_2$ series as one moves from $C_5H_5$ to $(CH_3)_4C_5H$ and to $Me_5C_5$ (Table 4). Note, however, that greater ring opening (smaller $\theta$) is observed in the dichlorides since two ligands effect greater crowding in the inter-ring region.

Metrical data for $Cp^{tt}_2TiCl$ and $Cp^{tt}_2TiCl_2$ offer generally consistent trends (Table 4) in this picture, with both the Ti−Cl and Ti−$Cp^{tt}$ centroid distances contracting for $Ti^{IV} \rightarrow Ti^{III}$. However, the 1,3-*tert*-butyl substitution in a nearly staggered ring conformation apparently requires unusual ring opening to accommodate the Cl ligation, while minimizing repulsion involving the massive *tert*-butyl substituents. Therefore, the 121° bending in $Cp^{tt}_2TiCl_2$ clearly reflects the pronounced steric demands versus simple methyl substitution. In less sterically encumbered $Cp^{tt}_2TiCl$, the $\theta$ angle is 134.8° and is more consistent with other data in the monochloride series (Table 4).

In accord with these considerations, computational evaluation of classical van der Waals energy contributions[21,39] yields comparative evidence of greater relative repulsive interactions in $Cp^{tt}$ complexes than in the unsubstituted analogues. Thus, the comparable computed van der Waals energies in all the $Cp^{tt}$ Zr and Ti derivatives (150−140 kcal/mol) can be contrasted with significantly reduced values in $Cp_2ZrI_2$ (92 kcal/mol) and $Cp_2ZrI$ (71 kcal/mol) and a remarkably smaller energy in $Cp_2TiCl_2$ (50 kcal/mol).

**Zr−I Bond Dissociation Enthalpy in $Cp_2ZrI_2$.** Calculation of the Zr−I bond dissociation enthalpy, D(Zr−I), was applied to the model process of eq 9. Any calculation on the real $Cp^{tt}$

$$Cp_2ZrI_2 \rightarrow Cp_2ZrI + I \qquad (9)$$

analogue including evaluation of correlation energies is far too computationally demanding, and, in any case, the direct electronic influence of *tert*-butyl ring substituents is not expected to be of major consequence as far as the D(Zr−I) is concerned. The calculated D(Zr−I) energy, at HF level of theory, is 33 kcal/mol and, as commonly encountered for other classes of similar compounds,[40] is underestimated with respect to experiment (58.0 kcal/mol). However, the inclusion of electron correlation effects, using the MP2 formalism, brings the calculated D(Zr−I) absolute value (64 kcal $mol^{-1}$) closer to experiment. The slight overestimation may be due to the simpler ligation model adopted.

## Discussion

The present study provides the first combined molecular structure, electronic structure, and absolute bonding energetic analysis of group 4 metallocene $\sigma$ bond homolysis processes. The metrical data (Table 4) and comparative van der Waals calculations argue that the scission process represented by $Cp^{tt}_2MI_2 \rightarrow Cp^{tt}_2MI + I$ is accompanied by substantial relaxation of repulsive interligand steric interactions. Examples are the ~0.06 Å *contraction* in M−$Cp^{tt}$ centroid distances for $Cp^{tt}_2MX_2 \rightarrow Cp^{tt}_2MX$ (M = Zr, X = I; M = Ti, X = Cl), whereas ionic radius considerations alone would predict an *expansion* of ~0.06 Å.[29] That the present experimental absolute $D[Cp^{tt}_2Zr(I)-I]$ value of 58.0(5) kcal/mol is in agreement with $D(I_3Zr-I) \approx 59$ kcal/mol argues that D(Zr−I) is transferable in this case, presumably because the steric and electronic environments are similar. However, that $D[Cp^{tt}_2Ti(I)-I]$ = 40.6(5) kcal/mol, while $D[(Me_5C_5)_2Ti(I)-I]$ = 52.3(6) kcal/mol and $D(I_3Ti-I)$ = 56(2) kcal/mol, suggests that metallocene vs $MI_4$ bond enthalpy deviations can be large in sterically congested situations. Requisite literature data are not available to calculate $D(I_3Hf-I)$; however, general trends are likely to be similar to those with Zr, judging from the numerous similarities in Zr(IV) and Hf(IV) bonding energetics.[1,2,10]

The trend in absolute metal−iodine bond enthalpies for the present group 4 metallocenes (Tables 11 and 16), $D[Cp^{tt}_2Hf(I)-I] > D[Cp^{tt}_2Zr(I)-I] > D[Cp^{tt}_2Ti(I)-I]$ exhibits the typical increase in D(M−X) upon descending a period, in agreement with other experimental data[1,2,4] and theoretical calculations for related group 4 metallocene alkoxide bonds.[41] As expected from previous studies of zirconocene and hafnocene alkyls,[10] the average Zr−Me and Hf−Me bond enthalpies are weaker than the corresponding metal−iodine bond enthalpies. The relative differences, $\bar{D}[(Cp^{tt}_2Zr(I)-I)] - \bar{D}[(Cp^{tt}_2Zr-Me_2)]$ = 15(2) kcal/mol and $\bar{D}[Cp^{tt}_2(I)Hf-I] - \bar{D}[Cp^{tt}_2Hf-Me_2]$ = 14(1) kcal/mol, are identical within experimental error to those for the sterically less encumbered $(Me_5C_5)_2MR_2$ (M = Zr, Hf) system,[10] $\bar{D}[(Me_5C_5)_2Zr(I)-I] - \bar{D}[(Me_5C_5)_2Zr-Me_2]$ = 13(2) kcal/mol and $\bar{D}[(Me_5C_5)_2Hf(I)-I] - \bar{D}[(Me_5C_5)_2Hf-Me_2]$ = 10(4) kcal/mol. The similarities in the relative metal−methyl to metal−iodide bond enthalpies suggest similarities in Me/I nonbonded interactions in $Cp^{tt}_2MR_2$ (M = Zr, Hf), reflecting, among other factors, similar methyl (2.00 Å) and iodine (1.90−2.12 Å) van der Waals radii.[26]

Table 16 compares the present absolute D(M−I) and D(M−Me) parameters with previous zirconocene and hafnocene results for $(Me_5C_5)$ and Cp ancillary ligation.[10] The earlier results were anchored to $\bar{D}(ZrCl_4)$ = 117 kcal/mol ≈ $D(Cl_3Zr-Cl)$ = 115.7 kcal/mol (taken from earlier compilations than are given in ref 31).[10] Note that the corresponding $D[Cp^{tt}_2M(X)-X] - D[(Me_5C_5)_2M(X)-X]/D[Cp_2M(X)-X]$ values are all on the order of 21−22 kcal/mol. While the foregoing structural discussion argues that a significant component of this bond weakening may reside in large, interligand cyclopentadienyl-based steric effects, note that ancillary halogen ligand effects on $D(MX_4)$ parameters are also significant for heavier halogens: $\bar{D}(ZrX_4) - D(X_3Zr-X)$ = 5.7(5) kcal/mol for X = Cl versus 24.5 kcal/mol for X = I.[31] Thus, while $\bar{D}[(Me_5C_5)_2Zr(I)-$

**Table 16.** Metal−Halogen/Methyl Bond Enthalpy Data for Selected Zirconocenes and Hafnocenes

| compound | $D(L_nM-L)$ kcal/mol |
|---|---|
| $(Me_5C_5)_2ZrI_2$[a] | $\bar{D}[L_nZr-I_2]$ = 80.4(5) |
| $(Me_5C_5)_2HfI_2$[a] | $\bar{D}[L_nHf-I_2]$ = 82(3) |
| $(Me_5C_5)_2ZrMe_2$[a] | $\bar{D}[L_nZr-Me_2]$ = 67(1) |
| $Cp_2ZrMe_2$[a] | $\bar{D}[L_nZr-Me_2]$= 67(1) |
| $(Me_5C_5)_2HfMe_2$[a] | $\bar{D}[L_nHf-Me_2]$ = 72(4) |
| $Cp^{tt}_2ZrI_2$ (**12**) | $D(L_n(I)Zr-I)$ = 58.0(5) |
| $Cp^{tt}_2HfI_2$ (**11**) | $D(L_n(I)Hf-I)$ = 61.2(4) |
| $Cp^{tt}_2ZrMe_2$ (**10**) | $\bar{D}[L_nZr-Me_2]$ = 43(1) |
| $Cp^{tt}_2HfMe_2$ (**9**) | $\bar{D}[L_nHf-Me_2]$ = 47.6(9) |

[a] Values are anchored to the corresponding $D(Cl_3M-Cl)$ (ref 10).

(38) Troyanov, S. I.; Rybakov, V. B.; Thewalt, U.; Varga, V.; Mach, K. *J. Organomet. Chem.* **1993**, *447*, 221.

(39) (a) Brubaker, G. R.; Johnson, D. W. *Coord. Chem. Rev.* **1984**, *53*, 1−36. (b) Hancock, R. D. *Prog. Inorg. Chem.* **1989**, *37*, 187−291.

(40) See, for example: (a) Sodupe, M.; Bauschlicher, C. W.; Langhoff, S. R.; Partridge, H. *J. Phys. Chem.* **1992**, *96*, 2118. (b) Bauschlicher, C. W.; Langhoff, S. R. *J. Phys. Chem.* **1991**, *95*, 2278. (c) Di Bella, S.; Lanza, G.; Fragalà, I. *J. Chem. Soc., Faraday Trans.* **1995**, *91*, 2709−2714.

(41) Ziegler, T.; Tschinken, V.; Versluis, L.; Baerends, E. J.; Ravenek, W. In ref 1b, pp 1625−1637.

I] = 80.4(5) kcal/mol (determined relative to $(Me_5C_5)_2ZrCl_2$[10]) is in good agreement with $\bar{D}(ZrI_4)$ = 83(1) kcal/mol,[31] it is in less good agreement with the aforementioned, less precise value of $D(I_3Zr-I)$, 59 kcal/mol.[31b] As noted above, this disparity is not so great for chlorides, where the latest compilations give $\bar{D}(ZrCl_4)$ = 117(1) kcal/mol and $D(Cl_3Zr-Cl)$ = 111.3(5) kcal/mol.[31] In sum, the lighter halogens are, at present, the less ambiguous anchor points for placing existing metallocene $\sigma$ bond enthalpies on an absolute scale, while heavier, more sterically encumbered halogens appear to be most reliable in sterically uncongested ancillary ligand environments, and their complexes warrant additional experimental bond enthalpy investigations. For thermochemically analyzing the great bulk of $L_2MX_2 \rightarrow L_2MY_2$ $\sigma$ bond transposition processes, these uncertainties should, of course, introduce no problems.

The diminution in metal−ligand bond enthalpies for metallocene systems containing sterically demanding ancillary ligands has interesting implications for reactivity. Weaker metal−ligand $\sigma$-bond enthalpies will favor lower oxidation states and increased exothermicity of reductive elimination processes. Estimated elimination processes involving some metallocene hydrocarbyls are shown in eqs 10−13.

Auxiliary data are taken from standard literature sources,[2] and estimated errors in calculated reaction enthalpies are ∼5 kcal/mol.

$$2(Me_5C_5)_2ZrMe_2 \rightarrow 2(Me_5C_5)_2ZrMe + Me-Me \quad (10a)$$

$$(Me_5C_5)_2ZrMe_2 \rightarrow (Me_5C_5)_2Zr + Me-Me \quad (10b)$$

$$\Delta H \approx +46 \text{ kcal/mol of Zr}$$

$$2(Me_5C_5)_2HfMe_2 \rightarrow (Me_5C_5)_2HfMe + Me-Me \quad (11a)$$

$$(Me_5C_5)_2HfMe_2 \rightarrow (Me_5C_5)_2Hf + Me-Me \quad (11b)$$

$$\Delta H \approx +56 \text{ kcal/mol of Hf}$$

$$2Cp^{tt}{}_2ZrMe_2 \rightarrow Cp^{tt}{}_2ZrMe + Me-Me \quad (12a)$$

$$Cp^{tt}{}_2ZrMe_2 \rightarrow Cp^{tt}{}_2Zr + Me-Me \quad (12b)$$

$$\Delta H \approx -2 \text{ kcal/mol of Zr}$$

$$2Cp^{tt}{}_2HfMe_2 \rightarrow Cp^{tt}{}_2HfMe + Me-Me \quad (13a)$$

$$Cp^{tt}{}_2HfMe_2 \rightarrow Cp^{tt}{}_2Hf + Me-Me \quad (13b)$$

$$\Delta H \approx +7.2 \text{ kcal/mol of Hf}$$

It can be seen that reductive elimination for the encumbered $Cp^{tt}{}_2MMe_2$ system is significantly favored over reductive elimination for the $(Me_5C_5)_2MMe_2$ system. In addition, the dimethylzirconocene systems favor reductive elimination over the dimethylhalfnocene complexes, in agreement with the slightly stronger hafnium−ligand bonds.

## Conclusions

Absolute M−I and $M-CH_3$ bond enthalpies have been measured for a series of $Cp^{tt}$-based group 4 metallocenes. These enthalpies increase on descending the Periodic Table and are depressed by the substantial steric crowding, the magnitude of which is confirmed by analysis of diffraction-derived metrical parameters, van der Waals computations, and ab initio quantum chemical computations. Sterically induced reduction of metallocene bond enthalpies significantly enhances the stability of lower oxidation states and should facilitate reductive elimination processes. These nonbonded interactions also affect the degree to which D(M−X) parameters can be transferred between metallocene and $MX_4$ ligation environments. Transferrability should be most reliable for lighter halogens in uncongested coordination spheres using $\bar{D}(MX_4)$ values.

**Acknowledgment.** This research was supported by the U.S. National Science Foundation (T.J.M., W.A.K., C.L.S.; Grant CHE9618589), the Ministero dell'Università e della Ricerca Scientifica e Tecnologica (I.L.F.; MURST Rome), and the Consiglio Nazionale delle Ricerche (I.L.F.; CNR, Rome).

**Supporting Information Available:** Complete list of atomic position and anisotropic thermal displacement parameters for $Cp^{tt}{}_2ZrI_2$, $Cp^{tt}{}_2HfI$, and $Cp^{tt}{}_2ZrI$; complete listing of bond distances and angles; tables of eigenvalues, and population analysis of $Cp_2ZrI_2$ with a $Cp_{centr}-Zr-Cp_{centr}$ of 126° and 133° bond angle; and He I/He II PE spectra of $Cp^{tt}{}_2ZrCl_2$ (20 pages, print/PDF). See any current masthead page for ordering information and Web access instructions.

JA9822815